Heat and Mass Transfer 38 (2002) 399–408 © Springer-Verlag 2001
DOI 10.1007/s002310100209

Experimental and numerical study of developing turbulent flow and heat transfer in convergent/divergent square ducts

L.-B. Wang, Q.-W. Wang, Y.-L. He, W.-Q. Tao

Abstract The work reported in this paper is a systematic experimental and numerical study of friction and heat transfer characteristics of divergent/convergent square ducts with an inclination angle of 1° in the two direction at cross section. The ratio of duct length to average hydraulic diameter is 10. For the comparison purpose, measurement and simulation are also conducted for a square duct with constant cross section area, which equals to the average cross section area of the convergent/divergent duct. In the numerical simulation the flow is modeled as being three-dimensional and fully elliptic by using the body-fitted finite volume method and the k–ε turbulence model. The uniform heat flux boundary condition is specified to simulate the electrical heating used in the experiments. The heat transfer performance of the divergent/convergent ducts is compared with the duct with uniform cross section under three constraints (identical mass flow rate, pumping power and pressure drop). The agreement of the experimental and numerical results is quite good except at the duct inlet. Results show that for the three ducts studied there is a weak secondary flow at the cross section, and the circumference distribution of the local heat transfer coefficient is not uniform, with an appreciable reduction in the four corner regions. In addition, the acceleration/deceleration caused by the cross section variation has a profound effect on the turbulent heat transfer: compared with the duct of constant cross section area, the divergent duct generally shows enhanced heat transfer behavior, while the convergent duct has an appreciable reduction in heat transfer performance.

Received on 18 September 2000 / Published online: 29 November 2001

L.-B. Wang[1], Q.-W. Wang, Y.-L. He, W.-Q. Tao (✉)
School of Energy and Power
Engineering Xi'an Jiaotong University Xi'an
Shaanxi 710049, China

Present address:
[1]Department of Mechanical Engineering
Lan Zhou Railway Institute
Lan Zhou, 730070, China

This work was supported by the Research Fund for the Doctoral Program of Higher Education of China (RFDP No. 9589801), the National Natural Science Foundation of China (No. 59806011) and the National Key Project of Fundamental R&D of China (Grant No. 2000026303).

List of symbols

A	area, m^2
A1, A2	inlet and outlet cross section area of duct, m^2
c_p	heat capacity, J/kg · K
C_p	pressure recover factor
D	hydraulic diameter, m
f	friction factor
h	heat transfer coefficient, W/m^2 · K
k	thermal conductivity, W/m · K, turbulent kinetic energy, $(m/s)^2$
L	axial length of duct, m
$\dot{m}$	mass flow rate, kg/s
Nu	Nusselt number
p	pressure, Pa
Δp	pressure drop of duct due to friction, Pa
Q	heat transfer rate, W
Q_{loss}	heat loss to environment, W
Re	Reynolds number
T	temperature, K
U	duct average velocity, m/s
x	streamwise direction, m
y, z	spanwise coordinates, m

Greek symbols

β	inclination angle, degree
ε	dissipation rate, $(m/s)^2$
ν	kinetic viscosity, m^2/s
ρ	fluid density, kg/m^3

Subscripts

b	bulk
in	inlet
m	mean
out	outlet
w	wall

1 Introduction

Ducts with rectangular cross section are widely used in the heat exchanger devices. Both laminar and turbulent developing and developed flows and heat transfer in rectangular ducts have been extensively studied. These results are well documented in references such as [1, 2]. However, cases are often encountered where a convergent and/or divergent duct with square cross section is adopted because of some technological or constructional demand. Examples include the heat exchanger located between the compression and expansion spaces of a Stirling cycle cryocooler [3], thrust chambers of cooled rocket engine,

and air intake ducts of fighter jet aircraft [4], etc. In addition, the convergent/divergent square ducts are also used in the modeling of gas turbine blade cooling process. The cooling channel of a gas turbine is often modeled by a duct with a square cross section [4]. In the flow direction, the cooling passages may vary its cross-section area. Such a geometric variation may induce some differences in both flow and heat transfer characteristics compared to those models with straight rectangular channel. The study on the effect of acceleration and deceleration of the turbulent flow on heat transfer in three dimensional ducts is of importance from either academic or engineering point of view.

The effect of the streamwise acceleration or deceleration on the development of turbulent boundary layer is of theoretical and practical significance, and have been extensively investigated [5–9]. The general conclusion obtained from these investigations about the effect of flow acceleration on turbulent heat transfer is that acceleration may lead to thermal boundary layer penetrating significantly beyond the velocity boundary layer and turbulent boundary layer may be laminarized, hence deteriorates the heat transfer. The focuses of these investigations were put on the boundary layer development and parabolic flow was usually employed. As far as the internal flow and heat transfer in three dimensional convergent/divergent ducts are concerned a search of literatures only revealed a limited number of publications, which are briefly reviewed as follows.

In the work of Tanaka et al. [10] heat transfer measurement was conducted for a fluid flow through a convergent to a constant cross section duct at Reynolds numbers ranging from 5000 to 14,000. The measured Nusselt numbers in the accelerating portion were less than constant area portion, suggesting laminarization. In the work of Mutama and Iacovides [11] the hydrodynamic and thermal development of turbulent boundary layers subjected to streamwise acceleration has been investigated in a long two-dimensional duct with the convergent angle being only 0.53°. The tested Reynolds number range is 4000–21,000. Their results show that even at so small acceleration parameter, the skin friction coefficients and Stanton number are well below those encountered in parallel channel flow at corresponding Reynolds numbers. The entry region behavior is further complicated by the combined effects of thin inlet boundary layer and streamwise acceleration.

As to the divergent duct, the flow has streamwise adverse pressure gradient. The divergent duct usually serve as a diffuser. Diffusers are widely used for converting kinetic energy to pressure. In the studies of diffusers, the main aim is to improve the efficiency of converting kinetic energy to pressure, and such studies of fluid flow in the diffusers had been carried out extensively. The study on heat transfer characteristics of divergent duct, however, is very limited, and the present authors only found one related paper by Su and Lin [12]. They conducted the numerical simulation of forced laminar convection in convergent and divergent ducts of rectangular cross section. The duct has constant height but its width varies along streamwise direction. The flow was modeled as being three-dimensional and parabolic, and the wall temperature was assumed to be constant. In their simulation the convergent (divergent) angle varied from 0 to 15° and the cross section aspect ratio varied from 1.0 to 0.1. The results show that increasing the convergent angle may significantly induce high temperature drop and Nusselt number. The total heat transfer, however, decreases because the decrease in heat transfer area. For the divergent ducts, Nusselt number is more or less the same for different divergent angles except in the entrance region. No any results of turbulent heat transfer were reported in the public literature.

The main objective of the present study is to discern the turbulent flow and heat transfer characteristics in convergent and divergent ducts. In this paper, the experimental and numerical methods are used to reveal the turbulent fluid flow and heat transfer characteristics in convergent and divergent square ducts with uniform heat flux boundary condition. In addition, the heat transfer behavior of the two ducts is compared with that of a uniform square duct under the constraints of identical pumping power, identical pressure drop and identical mass flow rate.

2 Experimental study

2.1 Experimental apparatus

A pictorial view of the test ducts are shown in Fig. 1. As shown in Fig. 1b, the same duct served as both convergent and divergent duct depending on the inflow direction. A schematic of the experimental setup is presented in Fig. 2. It is a suction system. A 3.5 kW blower was used to draw the air from the laboratory room to the test duct via a convergent inlet and a plenum, which is used to provide a sharp construction entrance condition. The test duct is connected to an after plenum and a transition duct whose cross-section gradually varies from square to circular. Connected to the transition duct is a tube with an inner diameter of 50 mm equipped with a multiport averaging Pitot tube [13] to measure flow rate.

Both uniform square-cross duct and convergent or divergent square-cross duct are designed and manufactured. The square duct has a cross section of 50×50 mm. The convergent/divergent square-cross duct has its largest cross-section of 58×58 mm and smallest cross-section of 41×41 mm. The test ducts both are 500 mm long in axial direction. These dimensions make the convergent/divergent duct has its two inclination angles $\beta_1 = \beta_2 \cong 1^\circ$ as schematically shown in Fig. 1c.

The ducts are wrapped uniformly by resistance strip which is controlled by a variac transformer to provide a controllable electrical heating to the test duct. The ducts are insulated by plastic foam. Forty eight copper-constantan thermocouples are used to measure the axial wall temperature distribution of one wall of each test duct. Since the effect of the natural convection can be neglected, one wall can be regarded as a representative of the others. These thermocouples are arranged in three axial lines, with one being the center line of the wall. Their axial positions are shown in Fig. 3a. For the three other walls without

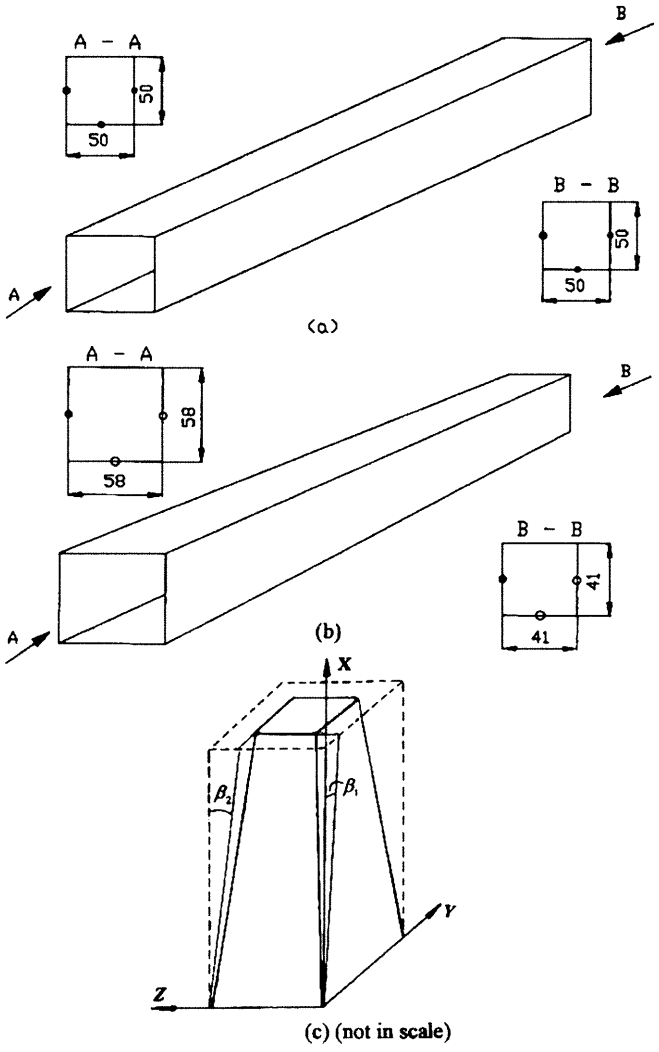

Fig. 1a–c. Schematic diagram of test ducts **a** square duct with constant cross section; **b** divergent/convergent square duct **c** pictorial view of inclination angle

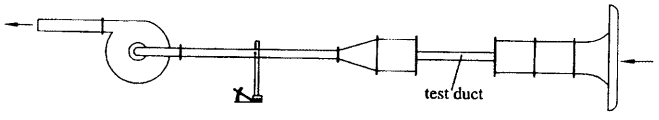

Fig. 2. Schematic diagram of test apparatus

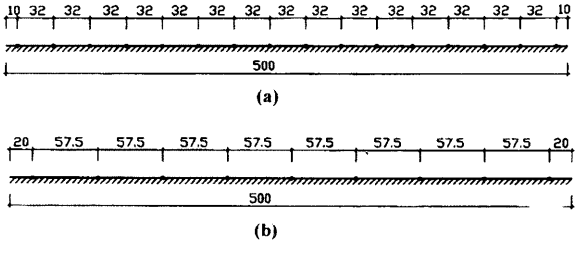

Fig. 3a, b. Arrangement of thermocouples and pressure taps **a** thermocouples; **b** pressure taps

thermocouples, nine pressure taps along the centerline of the each wall are used for static pressure drop measurement. Axial pressure tap locations are given in Fig. 3b. An incline manometer with an resolution of 1.63 Pa is used for pressure drop measurement in the test ducts. All the thermocouple signals are acquired with a data acquisition system and sent to a personal computer for data reduction. The temperatures of the entering fluid is measured by one thermocouple checked by a liquid thermometer with a resolution of 0.1 °C, while the leaving fluid temperature is measured by five thermocouples distributed at a screen set up adjacent to outlet section of the test duct.

2.2 Data reduction

The local heat transfer coefficient is calculated by the following equation:

$$h_x = (Q - Q_{\text{loss}})/[A(T_{\text{w},x} - T_{\text{b},x})] \tag{1}$$

where Q is the total thermal power supplied by the electrical heater, Q_{loss} is the power loss to the environment, A is the total inner surface area. The local wall temperature used in Eq. (1), $T_{\text{w},x}$, is obtained from the output of the average thermocouple readings at each cross-section.

The local bulk temperature used in Eq. (1) is calculated by the following equation

$$T_{\text{b},x} = T_i[(Q - Q_{\text{loss}})A_x]/(\dot{m}c_pA) \tag{2}$$

where A_x is the partial surface area of the duct from the inlet to the axial position x. The heat loss to the environment is estimated by heat conduction through the plastic foam and the two end losses. And for the most cases studied the ratio of Q_{loss}/Q is less than 5%. This estimation is confirmed by the thermal energy balance between the fluid enthalpy increase and the total power input. In the data reduction Q_{loss} is determined from the measured outlet fluid temperature.

The local Nusselt number is defined by

$$\text{Nu}_x = h_xD_{\text{m}}/k \tag{3}$$

The duct average Nusselt number and Reynolds number are defined by

$$\text{Nu} = (Q - Q_{\text{loss}})D_{\text{m}}/[kA(T_{\text{w}} - T_{\text{b}})], \quad \text{Re} = \frac{U_{\text{m}}D_{\text{m}}}{\nu} \tag{4}$$

The characteristic length, average bulk temperature and average wall temperature of the duct are defined by

$$D_{\text{m}} = \frac{D_{\text{in}} + D_{\text{out}}}{2}, \quad T_{\text{b}} = \frac{T_{\text{in}} + T_{\text{out}}}{2}, \quad T_{\text{w}} = \frac{1}{A}\int_0^A T_{\text{w},x}\,\text{d}A \tag{5}$$

In the data reduction, T_{b} is taken as the reference temperature and U_{m} is calculated by the duct midway cross section area.

Attention is now turned to the definition of the duct friction factor. For the constant cross-section duct, the average friction factor is defined by

$$f = [(\Delta p/L)D_{\text{m}})]/(\rho U_{\text{m}}^2/2) \tag{6}$$

where Δp is the pressure drop of the entire test duct due to friction.

As for the convergent or divergent duct, the definition of the friction factor should take the effect of the variation of the cross section into account [14, 15]. The average friction factor for the duct is defined by:

$$f = \frac{U_1^2}{U_m^2} \cdot \frac{D_m}{L} \lambda \left[1 - \left(\frac{A_{in}}{A_{out}} \right)^2 \right] \quad (7)$$

where λ is defined by

$$\lambda = 1 - C_p \quad (8)$$

In Eq. (8) C_p is the pressure recover factor for the entire test duct, which is defined as follows:

$$C_p = \frac{p_{out} - p_{in}}{\rho U_{in}^2/2} \quad (9)$$

The pressure drop data of the present investigation were measured for heated fluids.

Using the uncertainty estimation method of Kline and McClintock [16] and Moffat [17] the maximum uncertainty in the average Nusselt number and average friction factor are estimated to be less than 9 and 11%, respectively.

2.3 Numerical investigation

The numerical simulations are performed by solving fully elliptic 3-D Navier–Stokes equations in body-fitted coordinate system. The flow and heat transfer are assumed to be incompressible, and in steady-state.

The grid systems used in the calculation are generated by the multisurface algebraic method [18–20]. The schematic of the three grid systems used in the computations are shown in Fig. 4.

The governing equations in the computational space are discretized by using the control-volume method [21]. In this procedure the computational domain is descretized by a series of control volumes, and the governing equations are then integrated over a control volume. During the integration the profile approximations are made in each coordinate direction for the dependent variables, leading to a system of algebraic equation that can be solved in an iterative manner. The velocity pressure-velocity coupling is handled by the SIMPLE algorithm [21]. The collocation grid arrangement is used in the present study. To ensure the coupling between velocity and pressure the momentum interpolation of Rhie and Chow [22] is adopted to determine the interface velocity. To make the numerical solution be independent on the under relaxation factor, the relaxation factor is resumed to one before the momentum interpolation is used to determine the interface velocity [23].

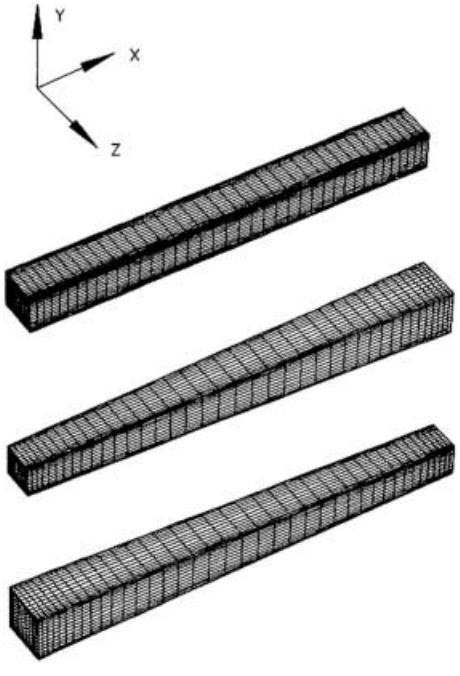

Fig. 4. Grid systems generated by multi-surface method

In the present calculation, the standard k–ε turbulent model is adopted [24]. The outlet boundary condition of the computational domain is treated by local one-way method [21]. The velocity and kinetic energy of turbulence are assumed to be uniform at the duct inlet. At the walls, the no-slip condition is used in conjunction with the wall functions method, which is implemented by the method provided in [25]. For temperature equation the wall functions are used to determine the wall temperature from the computed near wall temperature fields, since the heat flux is prescribed at the wall. The difference between the wall temperature so determined and the local bulk temperature is then used to compute the local heat transfer coefficient.

In the calculation, it was found that when the inlet k is in the range of 0.5–1.5% kinetic energy of flow, there is insignificantly effect on numerical results. The good agreement between numerical and experimental results was found when the y^+, z^+ are in the range of 11.5–40. Grid-independence studies were performed for case of $Re_m = 100,000$ to all three ducts, and results for grid sizes of $41 \times 16 \times 16$, $61 \times 16 \times 16$, $41 \times 21 \times 21$ were obtained. The difference between the results is less than 1%, then the solutions presented in this paper were obtained using the $41 \times 21 \times 21$ grid.

3 Results and discussion

In order to simplify the presentation, the following symbols are adopted for the three ducts: A-1: uniform cross-section square duct; A-2: divergent duct; A-3: convergent duct. For a concise presentation, the experimental and numerical results will be provided in a parallel way.

3.1 Local characteristics

The measured local heat transfer coefficients and pressure recover factors of the three ducts are presented in Figs. 5 and 6.

From Fig. 5, following features may be noted. First, as expected, for each of the tested ducts, the local heat transfer coefficient increases with the Reynolds number. Second, at the inlet of each tested duct, the local heat transfer coefficient decrease significantly along streamwise direction. Third, in the downstream part of the duct, the

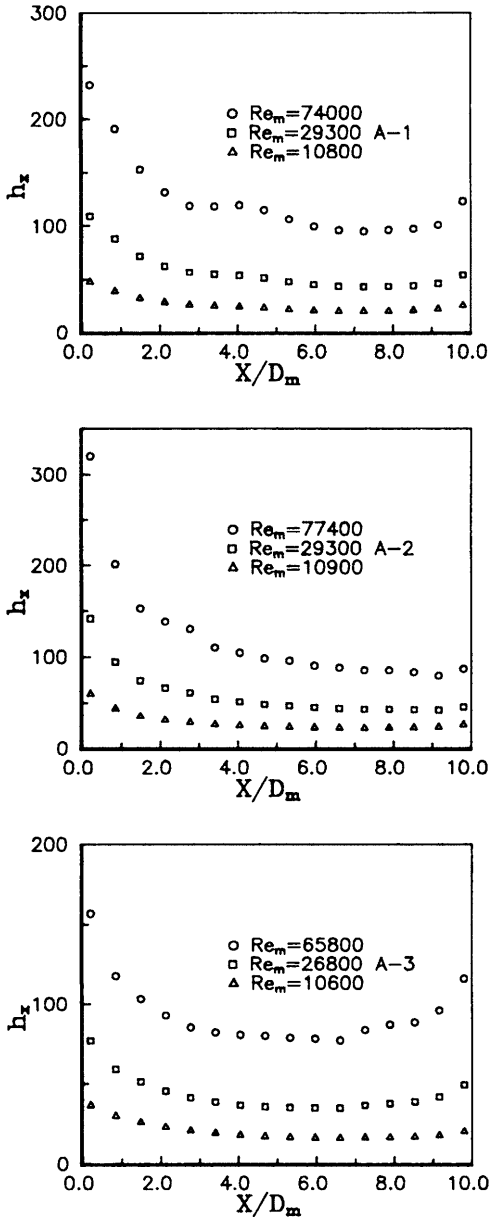

Fig. 5. Experimental local heat transfer coefficient

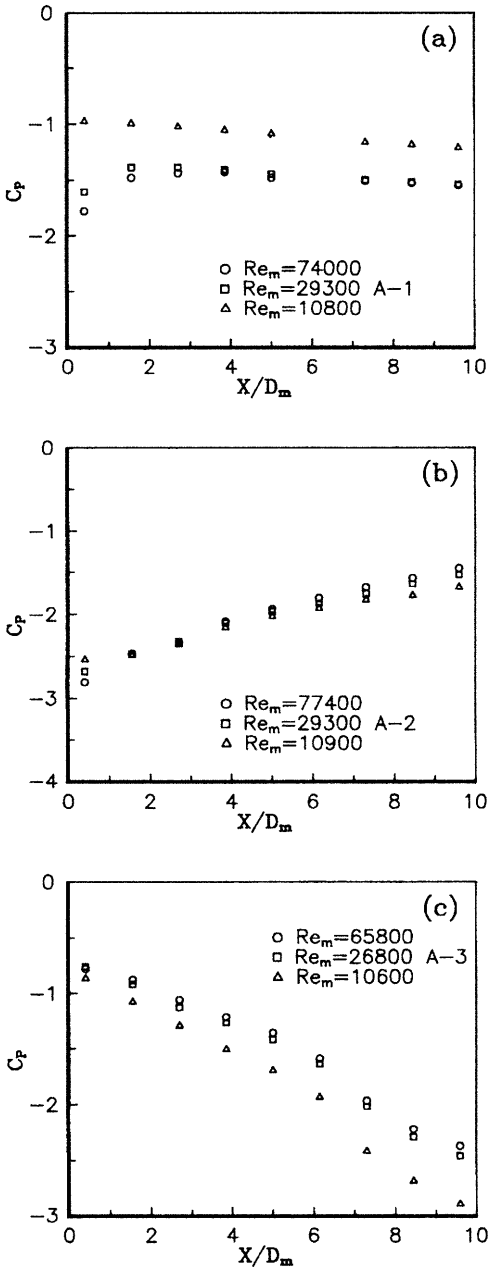

Fig. 6a–c. Experimental local pressure recover factor

streamwise variations of the local heat transfer coefficients are quite different. For the uniform cross section duct, h_x reaches a constant after x/D_m is greater than 6; while for the divergent duct a continuing decrease trend in the local heat transfer coefficient can still be observed, especially for the higher Reynolds number case. As for the divergent duct, the streamwise variation trend of h_x in this part is just opposite. And the higher the Reynolds number, the more appreciable the streamwise increase trend. It should be noted that in the three figures, the heat transfer measurement data of the last station all have a trend of increasing. This is expected to be resulted by the end heat loss, which make the wall temperatures nearby decrease in some extent. The guide-heating method should have been adopted to alleviate such phenomenon. To be objective, the data of the last stations for the three ducts are still retained in the pictures. The different streamwise variation trends of the local heat transfer coefficients for the three ducts are obviously caused by the streamwise acceleration or deceleration as revealed by previous investigation for two dimensional boundary layer flows.

The measured pressure recovery factors also represent the significant effect of the different streamwise duct shape. For the uniform cross-section duct the pressure drop is basically induced by skin friction. As can be seen from Fig. 6a along the streamwise direction, the absolute value of the pressure recovery factor decrease mildly in the most part of the duct. While for the divergent and convergent ducts, the pressure drop is mainly induced by the change in streamwise cross-section, which leads to the transformation between the dynamic and static pressures of fluid, resulting in streamwise increase (A-2) or significantly decrease (A-3) of C_p, as can be observed from Fig. 6b, c.

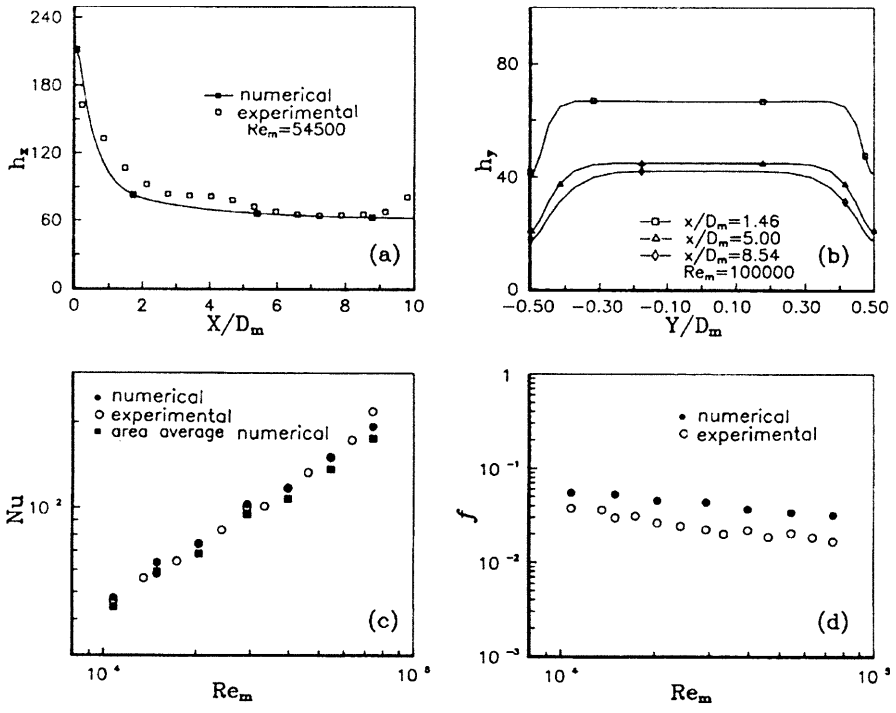

Fig. 7a–d. Numerical results of heat transfer coefficients and friction factor (duct A1)

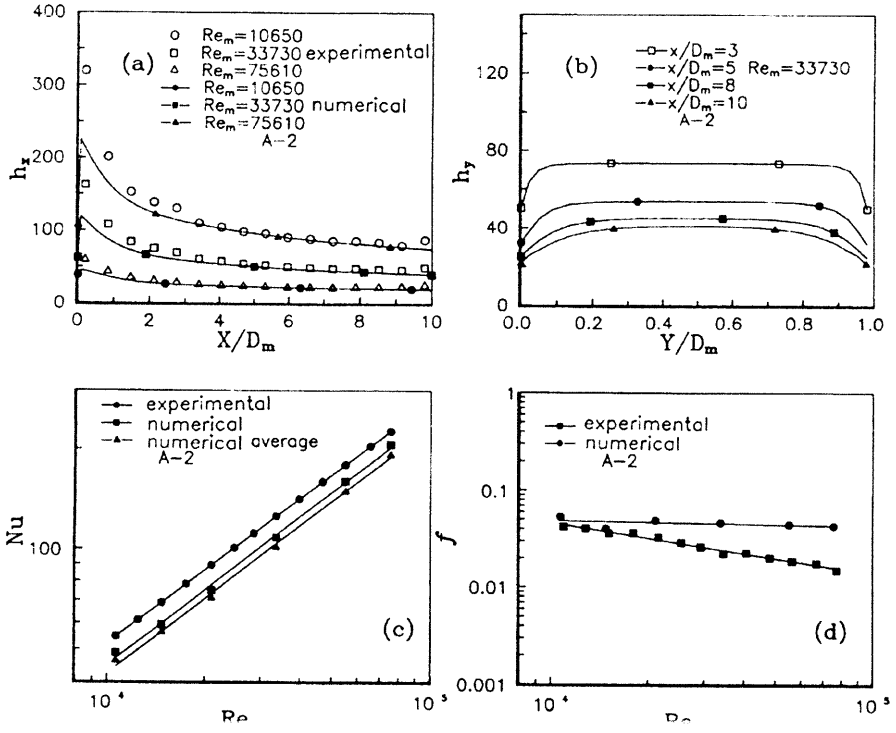

Fig. 8a–d. Numerical results of heat transfer coefficients and friction factor (duct A2)

The numerical results of local heat transfer characteristics are shown in Figs. 7a, b, 8a, b, 9a, b. As indicated by these figures, generally speaking, the agreement between the numerical results and experimental results is satisfactorily, except for the duct inlet where the discrepancy between the numerical and test data may be attributed to the inlet condition simulation. The spanwise local heat transfer coefficient distributions presented in Figs. 7b, 8b, 9b all show that in the duct corner, the heat transfer coefficient is relatively low compared to the other part of the wall. This is basically caused by the retarding effect of the corner walls which appreciably slows down the fluid velocity in the corner region, thereby deteriorates the local heat transfer.

Figure 10 shows the cross section velocity field in the middle section of the three ducts. It is found that for all the three ducts, the secondary flow at the cross section are all very weak. In the uniform cross section duct (Fig. 10a) and the convergent duct (Fig. 10c), the fluid moves from outside to inner core of the cross section, while in the

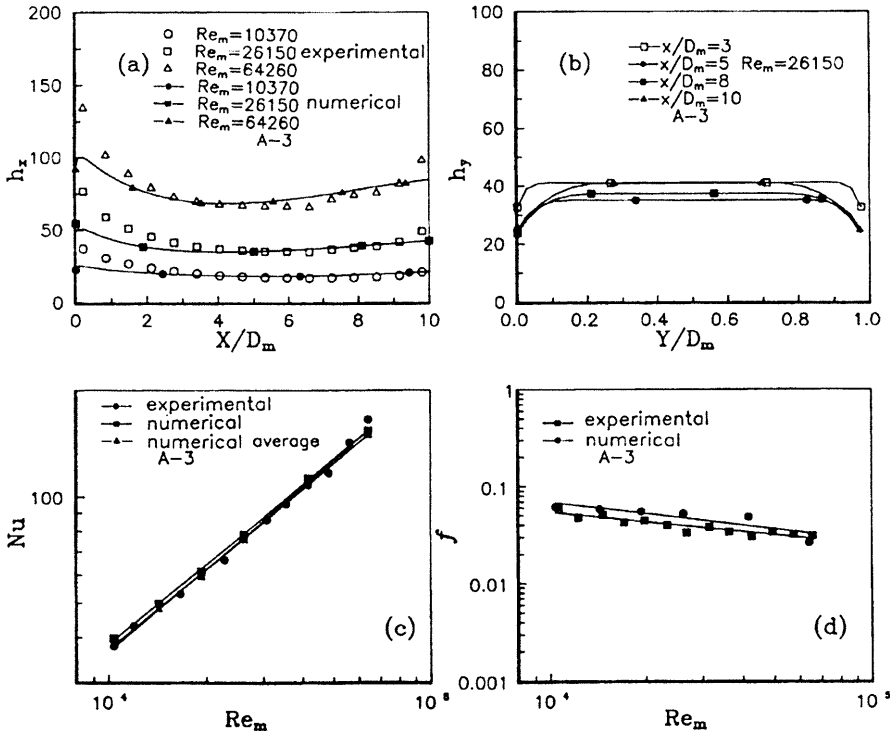

Fig. 9a–d. Numerical results of heat transfer coefficients and friction factor (duct A3)

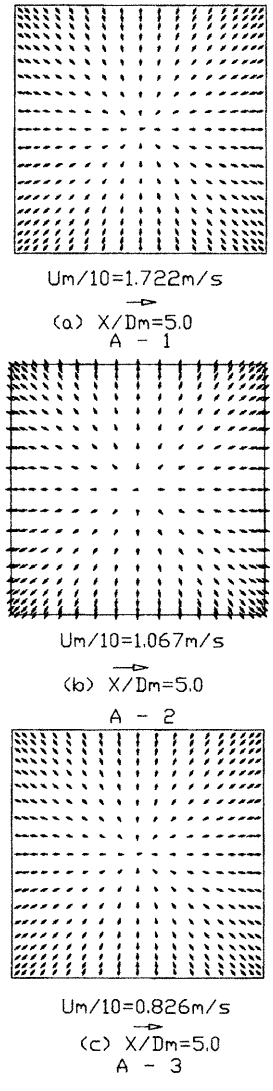

Fig. 10. Cross section velocity field

divergent duct the secondary flow is from the center to outside of the duct. These differences in the secondary flow are also induced by the different streamwise cross section variation pattern.

Attention is now turned to the average characteristics. The average Nusselt number of the wall centerline and duct friction obtained by experiments are presented in Fig. 11. The Dittus–Boelter equation is also plotted there for comparison. It can be seen that the average Nusselt number of A-1 is larger than the value calculated by the Dittus–Boelter equation. This is not surprising, because the Dittus–Boelter equation is for the fully developed region while the L/D_m of the tested ducts is only ten. In addition, presented in the figures are the centerline averaged Nusselt numbers which may be a bit higher than the surface averaged ones. Figure 11b, c show that the average Nusselt number of the divergent duct is appreciably greater than that predicted by the Dittus–Boelter equation, while that of the convergent duct exhibits inferior heat transfer behavior, reflecting the negative effect of the streamwise acceleration on the heat transfer in duct flow.

The friction factors of the three ducts are shown in Fig. 11d–f. The general variation trend of f with Re_m of the three ducts are the same, i.e., f decreases with the increase in Re_m. Carefully inspection, however, indicates that the rate of decreasing is different, with that of A-2 the fastest while that of A-3 the lowest. The acceleration and deceleration of flow in the convergent and divergent ducts make the skin friction has different characteristics. In divergent duct, the fluid velocity decreases along the flow direction, so does the skin friction. In convergent duct, the flow velocity increases along the flow direction, so increases the

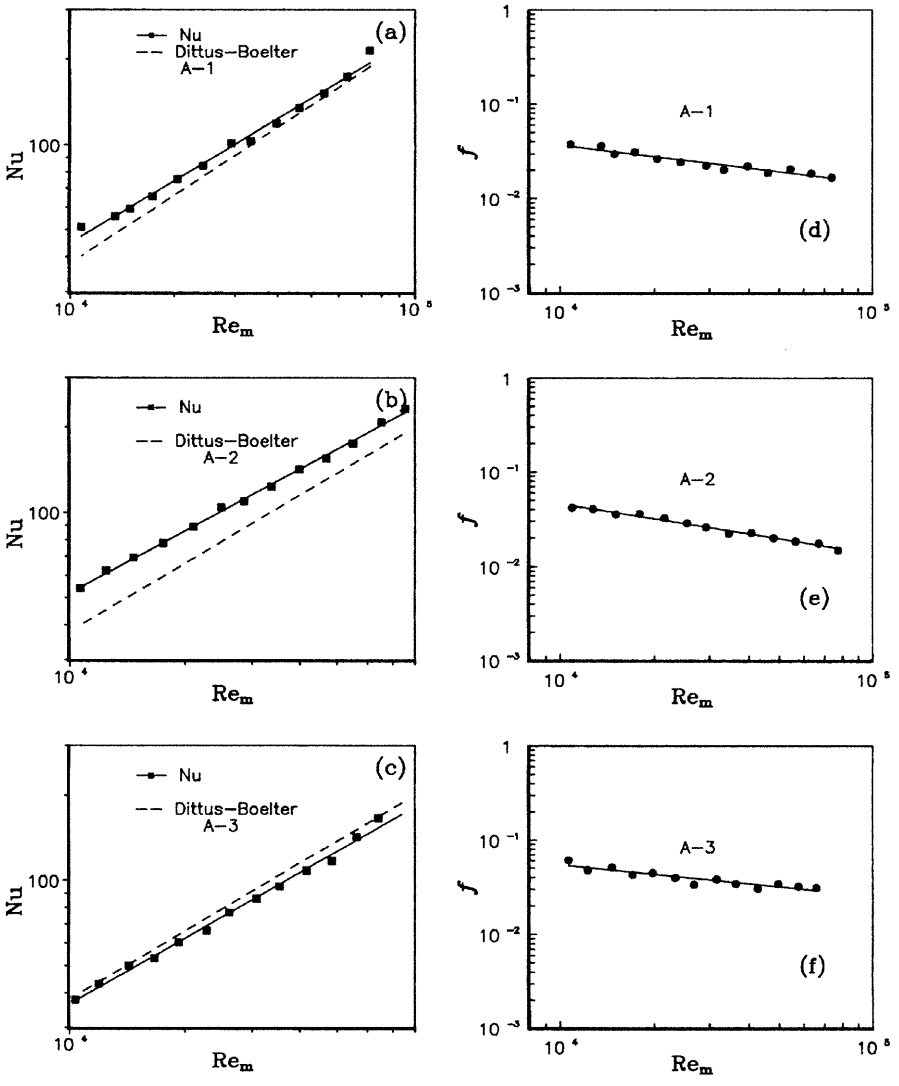

Fig. 11a–f. Experimental average Nusselt number and friction factor

skin friction. It is to be noted that the effect of the static pressure variation caused by the streamwise change in cross section area has been excluded in calculation of f.

The numerical results of the centerline average and surface average Nusselt number are shown in Figs. 7c, 8c and 9c. The numerical results of f are shown in Figs. 7d, 8d and 9d. It can be seen that for duct A-1 and A-3, the numerical results of centerline Nusselt number agree well with the experimental results. There also has a quite satisfactorily agreement between the numerical and experimental friction factor for the two ducts. For duct A-2, however, the discrepancy between the numerical and experimental results are a bit larger, with under-estimation of heat transfer and over-estimation of friction factor. This discrepancy may be attributed to the adopted standard k–ε turbulence model.

3.2
Heat transfer performance comparison

Attention is now turned to the relative heat transfer performance of divergent and convergent ducts with the uniform square ducts as a reference. The three widely used constraints are adopted: identical flow rate, identical pumping power, and identical pressure drop. Based on the constant property assumption and the same characteristic length, the formulations of the three constraints are given in the following:

(a) Identical mass flow rate

$$(\dot{m})^* = \dot{m} \tag{10a}$$

where the superscript "$*$" stands for the compared duct and the quantity without $*$ for the referenced duct. From Eq. (10a) we can obtain following relationship between the Reynolds number of the duct compared and the reference duct:

$$\mathrm{Re}_\mathrm{m}^* = \mathrm{Re}_\mathrm{m} D_\mathrm{m}^* / D_\mathrm{m} \tag{10b}$$

(b) Identical pumping power

$$\left(\frac{\dot{m}}{\rho}\Delta p\right)^* = \left(\frac{\dot{m}}{\rho}\Delta p\right) \tag{11a}$$

This leads to

$$\mathrm{Re}_\mathrm{m}^* = \sqrt[3]{\frac{Af\mathrm{Re}_\mathrm{m}^3}{(Af)^*}} \tag{11b}$$

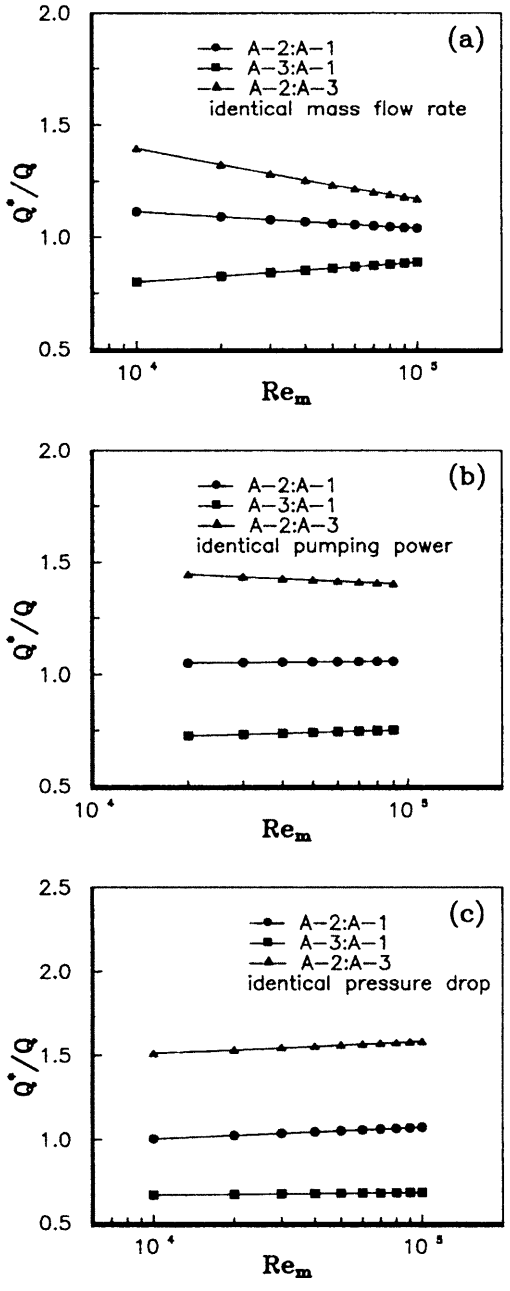

Fig. 12a–c. Heat transfer performance comparison

(c) Identical pressure drop

$$(fu^2)^* = fu^2 \tag{12a}$$

Then we have

$$\mathrm{Re}_\mathrm{m}^* = \mathrm{Re}_\mathrm{m}\sqrt{f/f^*} \tag{12b}$$

Under the condition of same temperature difference between the fluid and the wall, the ratio of heat transfer between the compared duct and the reference duct may be formulated as follows:

$$\frac{Q^*}{Q} = \frac{[A\mathrm{Nu}(\mathrm{Re}_\mathrm{m})]^*}{[A\mathrm{Nu}(\mathrm{Re}_\mathrm{m})]} \tag{13}$$

where $\mathrm{Nu}(\mathrm{Re}_\mathrm{m})$ represents the experimental correlation between Nusselt number and the Reynolds number, which are presented in Fig. 11.

The comparisons of the three ducts are shown in Fig. 12. It can be seen from Fig. 12a that under the identical mass flow rate constraint, the tested divergent duct may enhance heat transfer by about 10%, while he convergent duct reduces heat transfer by about 20% in average. Figure 12b shows that for the constraint of identical pumping power, the heat transfer enhancement of duct A-2 and deficit of A-3 are about 5 and 25%, respectively. The identical pressure drop is the most severe comparison constraint. As can be observed from Fig. 12c, the divergent duct has almost the same heat transfer rate as that of A-1, while the convergent duct deteriorates the heat transfer by 30%. Apart from the acceleration and deceleration effect of the divergent and convergent ducts, the surface area is the another ingredient that makes these two ducts behave so differently. As presented in Fig. 5, at the duct inlet, for each duct the local heat transfer coefficient is the highest. For the divergent duct the heat transfer area per unit axial length at the duct inlet is also the highest, while for the convergent duct it is the lowest, thus making the production of $A\mathrm{Nu}_\mathrm{m}$ different appreciably. In the three panels, the relative comparisons of A-2 to A-3 under the three constraints are also presented, with a ratio being always larger than 1.0.

4 Concluding remarks

The work reported here is a systematic experimental and numerical study of heat transfer and friction factor of a divergent/convergent duct with inclination angle of 1° in y- and z-directions. In the experimental study, the local heat transfer coefficient and the pressure recover factor were measured for air flowing in the divergent, convergent and uniform cross section ducts. The Reynolds number variation range was 10^4–8×10^4. In the numerical simulation the flow is modeled as being three-dimensional and fully elliptic by using the body-fitted finite volume method with uniform surface heat flux. The k–ε two-equation turbulence model in conjunction with the wall function method was adopted. In the paper both the local and average heat transfer and pressure drop characteristics are presented in detail. The agreement between test data and the numerical results is satisfactorily, except for the duct inlet. Numerical simulation revealed that for the three ducts simulated the heat transfer coefficient in the duct corner region is appreciably lower than that of other part of the duct wall, and there is a weak secondary flow at the cross section. The heat transfer performance comparison of the convergent/divergent ducts with the constant cross section duct were also conducted. The results show that even with only 1° inclination the divergent duct generally show favorite behavior in heat transfer while the convergent duct definitely exhibits inferior heat transfer performance. This implies that the streamwise acceleration/deceleration has a profound effect on the heat transfer for the three dimensional turbulent flow in ducts.

References

1. **Shah RK; London AL** (1978) Laminar Forced Convection in Ducts, Advances in Heat Transfer, Supplement. Academic Press, San Diego

2. **Ebadiab MA; Dong ZF** (1998) Forced convection, internal flow in ducts. In: Rohsenow WM, Hartnett JP, Cho YI (eds) Handbook of Heat Transfer, 3rd edn. McGraw-Hill, New York
3. **Hutchinson AC** (1982) Steady Flow Examination of a Cryocooler, Proc. 17th Int. Society of Energy Conversion Engineering Conference, 1850–1982
4. **Han JC** (1988) Heat transfer and friction characteristics in rectangular channels with rib turbulators. ASME J Heat Transfer 110: 321–328
5. **Launder BE** (1964) Laminarization of the turbulent boundary layer in a severe pressure gradient. ASME J Appl Mech 31: 707–708
6. **Patel VC; Head MR** (1968) Reversion of turbulent to laminar flow. J Fluid Mech 34(2): 371–392
7. **Launder BE; Lockwood FC** (1969) An aspect of heat transfer in accelerating turbulent boundary layers. ASME J Heat Transfer 91: 229–234
8. **Kays WM; Moffat RJ; Thieelbahr WH** (1970) Heat transfer to the highly accelerated turbulent boundary layer with and without mass addition. ASME J Heat Transfer 92: 468–475
9. **Succec J; Lu Y** (1990) Heat transfer across turbulent boundary layers with pressure gradients. ASME J Heat Transfer 112: 906–912
10. **Tanaka H; Kawamura H; Tateno A; Hatamaya S** (1982) Effects of laminarization and retransition on heat transfer for low Reynolds number flow through a converging to a constant area. ASME J Heat Transfer 104: 363–370
11. **Mutama KR; Iacovides H** (1993) The investigation of developing flow and heat transfer in a long converging duct. ASME J Heat Transfer 115: 897–903
12. **Su CC; Lin H** (1991) Forced convection in convergent and divergent ducts of rectangular cross section. Num Heat Transfer, Part A 20: 445–458
13. **Miller RW** (1996) Flow Measurement Engineering Handbook, 3rd edn. McGraw-Hill, New York
14. **Ward-Smith AJ** (1980) Internal Fluid Flow. Oxford University Press, Oxford, pp 195–247
15. **Wang LB** (1996) Experimental and Numerical Study of Turbulent Fluid Flow and Heat Transfer in Sectionally Complex and Twisted Ducts. Ph.D Thesis, Xi'an Jiaotong University, Xi'an, China
16. **Kline SJ; McClintock FA** (1953) Describing uncertainties in single-sample experiments. Mech Eng 75: 3–8
17. **Moffat RJ** (1988) Describing the uncertainties in experimental results. Exp Ther Fluid Sci 1: 3–17
18. **Eiseman PR** (1979) A multi-surface method of coordinate generation. J Comput Phys 33: 118–150
19. **Eiseman PR** (1982) Coordinate generation with precise controls of mesh properties. J Comput Phys 47: 330–351
20. **Eisemann PR** (1982) High level continuity for coordinate generation with precise controls. J Comput Phys 47: 352–374
21. **Patankar SV** (1980) Numerical Heat Transfer and Fluid Flow, Hemisphere Publishing Co., New York
22. **Rhie CM; Chow WL** (1983) Numerical study of the turbulent flow past an airfoil with trailing edge separation. AIAA J 21: 1525–1532
23. **Melaaen MC** (1992) Analysis of fluid flow in constructed tubes and ducts using body-fitted non-staggered grids. Int J Num Meth Fluids 15: 895–923
24. **Launder BE; Spalding DB** (1974) The numerical computation of turbulent flows. Comp Meth Appl Mech Eng 3: 269–289
25. **Tao WQ** (1988) Numerical Heat Transfer, Xi'an Jiaotong University Press, Xi'an, China